DOI: https://doi.org/10.62985/j.huit_ojs.vol25.no2.188

GREEN SYNTHESIS OF SILVER NANOPARTICLES FROM *Chrysanthemum morifolium* EXTRACT: EFFECTS OF pH, ANTIBACTERIAL, AND ANTIFUNGAL ACTIVITIES

Pham Ngoc Bao Tram, Nguyen Quoc Tuan, Huynh Phuoc Thong, Nguyen Thi Luong, Le Thi Hong Thuy*

Ho Chi Minh City University of Industry and Trade

*Email: *thuylth@huit.edu.vn*

Received: 3 March 2025; Accepted: 9 April 2025

ABSTRACT

This study investigates the effect of pH on the synthesis of silver nanoparticles (AgNPs) using *Chrysanthemum morifolium* extract (CFE) as a reducing agent, and evaluates their antibacterial and antifungal activities at the optimal pH condition. The UV-Vis spectra displayed a characteristic surface plasmon resonance (SPR) peak at 405–411 nm, with the most intense absorption occurring at pH 11. Dynamic light scattering (DLS) measurements revealed that nanoparticles synthesized at pH 10–11 exhibited the smallest hydrodynamic diameter (10.156–10.666 nm) and a polydispersity index (PDI) below 0.3, ensuring high stability and uniformity. TEM and XRD analyses revealed that the AgNPs exhibited a uniform spherical morphology and a face-centered cubic (FCC) crystal structure, with an average crystallite size of 10.021 nm. AgNPs demonstrated strong antibacterial activity against *Staphylococcus aureus* and antifungal activity against *Candida albicans*, which are two common pathogens associated with skin and mucosal infections. These results highlight the potential of AgNPs for applications in medical, pharmaceutical, and cosmetic products.

Keywords: Silver nanoparticles, *Chrysanthemum morifolium*, green synthesis, antibacterial activity, antifungal activity.

1. INTRODUCTION

In recent decades, noble metal nanoparticles have attracted significant attention from researchers due to their remarkable antibacterial properties, primarily attributed to their high surface-to-volume ratio, which enhances their ability to inhibit bacteria, resist antibiotics, and control the growth of drug-resistant strains [1]. Among these nanomaterials, silver nanoparticles (AgNPs) have established themselves as the flagship product of nanotechnology due to their unique physicochemical and biological properties. They are highly valued for their chemical stability, excellent electrical conductivity [2], catalytic activity, and antibacterial [3], antiviral [4], and antimicrobial properties [5]. Due to the size effect, AgNPs have widespread applications in biomedicine, drug delivery, antibacterial agents, water treatment, and agriculture. The antibacterial properties of AgNPs play a critical role in treating infections, especially as antibiotic resistance among bacteria becomes increasingly severe [6, 7].

Several methods have been explored for the synthesis of AgNPs, including chemical, physical, and biological approaches [8]. Among these, chemical reduction remains the most widely used due to its efficiency in rapidly generating large quantities of nanoparticles. However, this method is hindered by its reliance on toxic reagents and the production of environmentally hazardous by-products [1]. In contrast, green synthesis via biological methods - which utilize natural reducing agents from plant extracts [9], bacteria [10], or fungi [11] - has emerged as a safe, cost-effective, and easily scalable alternative [12, 13]. In particular, synthesizing AgNPs using plant extracts not only streamlines the process by eliminating the complexities of cell culture but also lends itself well to industrial-scale production, yielding nanoparticles with average sizes ranging from 5 to 90 nm and excellent biocompatibility [14, 15]. Several plant extracts, such as those from turmeric (*Curcuma longa* L.) [16],

sweet orange peel (*Citrus sinensis*) [17], tea leaves (*Camellia sinensis*) [18], and okra flower (*Abelmoschus esculentus*) [19], have been explored for AgNPs synthesis.

Chrysanthemum, particularly Chrysanthemum morifolium, is a genus within the family Asteraceae that comprises nearly 300 species distributed worldwide. Notably, East Asia-including China, Japan, Korea, and Siberia-harbors about 40 *Chrysanthemum* species, with China and Japan considered centers of biodiversity for this genus. The *Chrysanthemum* is integral to natural ecosystems and holds significant value in horticulture and medicine [20, 21]. Its extracts, rich in bioactive compounds such as polyphenols [22], flavonoids [23], and terpenoids [24], serve as potent reducing and stabilising agents in the green synthesis of silver nanoparticles. They play a crucial role in facilitating the reduction and stabilisation of AgNPs during green synthesis [25]. Numerous studies have utilised *Chrysanthemum* extracts to synthesise AgNPs with varied particle sizes. For instance, *Chrysanthemum morifolium* R. (20–50 nm) [26], *Chrysanthemum indicum* L. (37.71–71.99 nm) [27], and *Chrysanthemum coronarium* (5–50 nm) [28]. These studies mainly focused on elucidating the role of bioactive compounds present in chrysanthemum flower extracts in reducing silver ions and stabilising silver nanoparticles. The obtained AgNPs were characterised by standard techniques such as UV-Vis, TEM, XRD and FTIR, and the antibacterial and antifungal activities of these silver nanoparticles were also evaluated [25–28]. Most studies have not yet focused on the effect of pH on the synthesis of AgNPs. Although some recent studies have mentioned the role of pH, most of the focus has been on other factors, such as silver nitrate ($AgNO_3$) concentration and reaction time. In contrast, the effect of pH has not been comprehensively studied [29, 30]. Therefore, this study presented the results clarifying the effect of pH on the formation and AgNPs when using Chrysanthemum morifolium extract as a reducing agent. In addition, the study will also evaluate the crystal structure and antibacterial and antifungal activities of the synthesised AgNPs. The results obtained from this study are expected to significantly contribute to the development of safe and effective nanomaterials, opening up potential application opportunities in biomedicine and environmental protection.

2. MATERIALS AND METHODS

2.1. Materials

Silver nitrate ($AgNO_3$, ≥99%, CAS-No: 7761-88-8), sodium hydroxide (NaOH, ≥98%, CAS-No: 1310-73-2), and polyvinyl alcohol (PVA, ≥98%) were purchased from Xiong Scientific (China). The *Chrysanthemum morifolium* used in this study was obtained in a dried and compressed form from Thao Duoc Viet Co., Ltd., and stored in a dry, well-ventilated environment before extraction. The main chemical composition of *Chrysanthemum morifolium*, expressed as a percentage of dry weight, includes moisture content (12.5%), ash content (2.48%), and crude fiber (12.80%). The total flavonoid content was 69.55 mg RE/100 g dry weight, while the total phenolic content was 106.49 mg GAE/100 g dry weight. Double-distilled water was used for the preparation of plant extracts and silver nitrate solutions.

2.2. Preparation of *Chrysanthemum morifolium* flowers extracts (CFE)

The CFE was prepared according to the method of Briliantama et al., with some modifications. Dried *Chrysanthemum morifolium* flowers were finely ground and stored in an airtight container before extraction. A precise amount of 10 g of dried flower powder was weighed and mixed with 100 mL of an ethanol-water mixture (20:80 v/v) in an Erlenmeyer flask. The mixture was subjected to ultrasonic treatment at 50 kHz, maintaining a temperature of 50 °C for 20 minutes to optimize the extraction of bioactive compounds. The extract was then filtered through Whatman No. 1 filter paper to remove solid residues and centrifuged at 5000 rpm for 15 minutes to obtain a clear extract. The resulting extract was concentrated using a rotary evaporator at 45 °C under reduced pressure and stored at 4 °C for silver nanoparticle synthesis [31].

2.3. Green synthesis of silver nanoparticles using CFE

Silver nanoparticles (AgNPs) were synthesized following the green synthesis method described by Popov et al., with modifications. A 5.0 mM silver nitrate ($AgNO_3$) solution was prepared and gradually introduced dropwise into 90 mL of Chrysanthemum morifolium extract containing 1 g/L polyvinyl alcohol (PVA) under continuous stirring. The pH of the reaction mixture was adjusted to 5, 6, 7, 8, 9, 10, 11, and 12 using 0.1 M NaOH solutions. The mixture was then subjected to ultrasonic

treatment in a water bath at 50 °C for 120 minutes to enhance nanoparticle formation. After ultrasonic treatment, the reaction mixture was transferred to a magnetic stirrer and continuously stirred at room temperature for 12 hours, with the vessel covered in aluminum foil to prevent unwanted photochemical reactions. A visible color change from light yellow to reddish-brown indicated the formation of AgNPs [32]. The synthesized silver nanoparticles (AgNPs) were purified by centrifugation at 8000 rpm for 15 minutes, followed by three washes with deionized water and ethanol to remove any unreacted components. The purified AgNPs were then vacuum-dried at 80 °C for 3 hours to obtain a fine powder. Finally, the dried nanoparticles were stored in a desiccator for further physicochemical characterization using transmission electron microscopy (TEM), X-ray diffraction (XRD), and dynamic light scattering (DLS) [28].

2.4. Silver nanoparticle characterization

UV–VIS spectroscopy

The optical properties of synthesized silver nanoparticles (AgNPs) were analyzed using ultraviolet-visible (UV-Vis) spectroscopy. The absorption spectra were measured with a UV-Vis spectrophotometer (JASCO V-730, Japan) across a wavelength range of 300–800 nm. The AgNP solution was diluted 100 times with deionized water. The characteristic surface plasmon resonance (SPR) peak of AgNPs was identified based on the maximum absorption wavelength (λ_max). All measurements were conducted at room temperature (25 °C) in quartz cuvettes featuring an optical path length of 1 cm.

TEM

The morphological characteristics and surface structure of AgNPs were analyzed using transmission electron microscopy (TEM, FEI Tecnai G2 20 S-TWIN, USA). A small amount of AgNP suspension was drop-cast onto a carbon-coated copper grid and allowed to dry at room temperature before imaging.

Particle size distribution analysis

The particle size distribution of AgNPs was determined using DLS analysis with the SZ-100 Horiba particle size analyzer (Horiba, Japan). The hydrodynamic diameter and polydispersity index (PDI) of AgNPs were recorded to evaluate their size distribution and colloidal stability.

X-ray diffraction (XRD)

The crystal structure and size of AgNPs were analyzed using an X-ray diffraction (XRD) system (XRD-SIEMENS Rotan, Germany). AgNPs powders were spread evenly on the sample holder, and diffraction patterns were recorded in the 2θ range of 10°–80° using Cu-Kα radiation (λ = 1.5406 Å) at an operating voltage of 40 kV and a current of 30 mA. The scanning rate was set at 0.02°/s. The crystallite size of AgNPs was estimated using the Debye-Scherrer equation:

$$D = \frac{K \cdot \lambda}{\beta \cdot \cos\theta}$$

where D is the crystallite size (nm), K is the Scherrer constant (0.95), λ is the X-ray wavelength (1.5406 Å), β is the full width at half maximum (FWHM) of the most intense diffraction peak, and θ is the Bragg angle (in degrees) [8].

2.5. Antibacterial and antifungal activity of AgNPs against *S. aureus* and *C. albicans*

The antibacterial activity against *S. aureus* and antifungal activity against *C. albicans* of AgNPs were evaluated using the agar well diffusion method, based on the protocol of Bishoyi et al. with some modifications. Sterile Mueller-Hinton Agar (MHA) plates were inoculated with *S. aureus*. In contrast, sterile Sabouraud Dextrose Agar (SDA) plates were inoculated with *C. albicans* from microbial suspensions standardized to a 0.5 McFarland standard. Wells with a diameter of 6 mm were aseptically created in the agar and filled with 100 µL of AgNPs solutions at concentrations of 25 ppm and 100 ppm. The plates were incubated for 24 hours at 37 °C for *S. aureus* and 30 °C for *C. albicans*. Antibacterial and antifungal activities were assessed by measuring the diameter of the inhibition zones (mm). Deionized water was used as a negative control, while Chloramphenicol (25 ppm) was a positive control for *S. aureus*, and Fluconazole (25 ppm) was a positive control for *C. albicans* [33].

3. RESULTS AND DISCUSSION

3.1. Formation of silver nanoparticles

The formation of silver nanoparticles (AgNPs) was assessed using UV-Vis spectroscopy (Figure 1) and direct visual observation of color changes in the solution (Figure 2). The UV-Vis spectrum results (Figure 1) indicate that CFE(2) shows strong absorption in the range of 320-380 nm, likely due to the presence of flavonoid and polyphenol compounds in the extract [34]. The $AgNO_3$ solution (1) does not exhibit any significant absorption peak in the 300-700 nm range, suggesting that silver ions remain in their free state. The emergence of a surface plasmon resonance (SPR) peak at 408 nm of AgNPs solution (3), confirms the formation of silver nanoparticles. The bioactive compounds in the CFE serve as reducing agents for silver ions and act as stabilizers, preventing nanoparticle aggregation. This phenomenon has been extensively documented in studies on the green synthesis of AgNPs using plant-based sources [35]. This characteristic absorption aligns with previous studies on the green synthesis of AgNPs utilizing plant extracts as reducing agents [36, 37]. The color change in the solution (Figure 2) also provides clear visual evidence of AgNPs synthesis. The initial $AgNO_3$ solution is colorless, while the CFE solution appears light yellow due to the presence of bioactive plant compounds. Following the synthesis reaction, the AgNPs solution turns dark brown, a distinctive characteristic of silver nanoparticles resulting from localized surface plasmon resonance effects [4]. This finding corresponds with the study by Singh et al. (2020), which indicated that AgNPs synthesized from plant extracts exhibited a similar color change and an absorption peak in the 400-420 nm range [38].

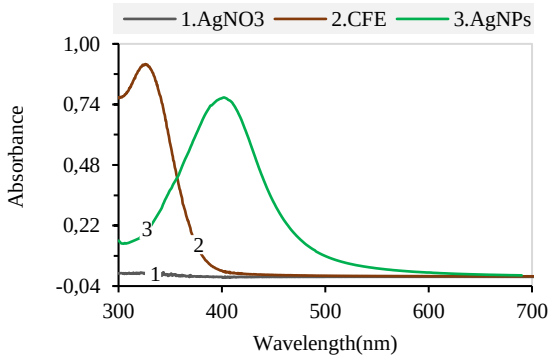

Figure 1. UV-Vis spectroscopy of $AgNO_3$(1), CFE(2), and AgNPs(3) at pH10 value

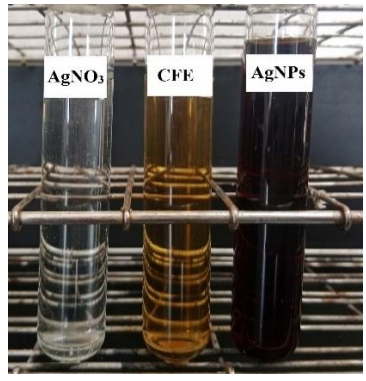

Figure 2. Appearance of $AgNO_3$(1), CFE(2), and AgNPs solution(3)

3.2. Influence of pH on maximum absorbance

Figure 3 presents the UV-Vis spectra of AgNPs synthesized at different pH values. The results show that changes in the intensity and position of the SPR peak reflect the influence of pH on nanoparticle size and distribution in the solution. In acidic (pH 5) and neutral (pH 7) environments, the absorption intensity is very low, and the SPR peak does not fall within the 400–420 nm range, indicating ineffective AgNPs formation. This may be due to both environments being unfavorable for the ionization of hydroxyl groups in CFE, reducing its ability to convert Ag^+ ions into Ag^o [39]. As the pH increases to 8–12, the absorption spectra become more distinct, demonstrating the formation of uniform AgNPs. The increase in pH facilitates the reduction of silver ions, as polyphenols and flavonoids in the extract can more easily release electrons [40]. The highest absorption intensity is observed at pH 11, indicating the highest efficiency in AgNPs synthesis. This could be attributed to the enhanced reducing power of the *Chrysanthemum* extract, which also generates electrostatic repulsion that stabilizes the nanoparticles in the solution, preventing aggregation [41]. However, when the pH further increases to 12, the absorption intensity decreases, possibly due to nanoparticle aggregation caused by reduced electrostatic repulsion, leading to the formation of larger AgNP clusters [42].

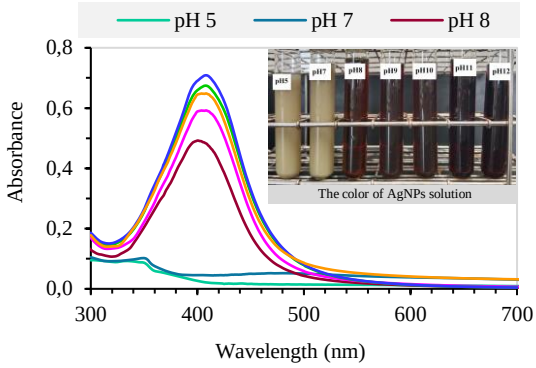

Figure 3. UV–Vis spectra and color of AgNPs at different pH values

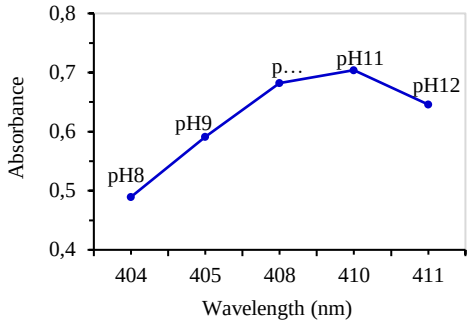

Figure 4. Relationship between wavelength and maximum absorbance at different pH values

The relationship between pH and the maximum absorption wavelength, as shown in Figure 4, reveals that as pH increases, the absorption peak shifts from ~405 nm to ~411 nm, indicating a slight increase in AgNPs size [43]. However, at pH 12, the maximum absorption decreases slightly, likely due to nanoparticle aggregation, which alters the morphology and size distribution of the AgNPs [39]. This result aligns with previous studies, where high pH values (>11) often lead to nanoparticle aggregation due to an imbalance between electrostatic repulsion and Van der Waals interactions [40, 44]. Therefore, the optimal conditions for synthesizing uniformly distributed and stable AgNPs are in the pH range of 10–11. At lower pH levels, silver ion reduction is limited, whereas, at excessively high pH, aggregation occurs, reducing the quality of the AgNP product.

3.3. Influence of pH on size distribution

The data presented in Figure 5 and Table 1 indicate that pH significantly affects the Z-average diameter and polydispersity index (PDI) of AgNPs, consistent with previous studies on pH-dependent nanoparticle synthesis [40, 41]. At pH 8, AgNPs exhibit a relatively larger size (11.850 nm) with a PDI of 0.321, which is slightly above the threshold for a monodisperse system. Despite high PDI, the size distribution pattern remains single-mode, suggesting that AgNPs at this pH behave similarly to those formed at pH 9–11. At pH 9–11, AgNPs demonstrate a smaller average size (10.156–11.101 nm) and PDI values below 0.3 (ranging from 0.273 to 0.284), indicating a stable and monodisperse system. This is explained as follows: In an alkaline environment, as the pH increases, the hydroxyl groups on the phenol rings of polyphenols and flavonoids are readily deprotonated to form phenolate ions ($-O^-$) with enhanced electron-donating ability. This process significantly increases the reducing power of these compounds, thereby facilitating the reduction of Ag^+ to Ag^0 and rapidly promoting the formation of silver nanoparticles. Moreover, with a high pH, the electrostatic repulsion between the phenolate ions becomes more vigorous, which helps prevent the aggregation of nanoparticles, resulting in better dispersion and more stable particle sizes [42].

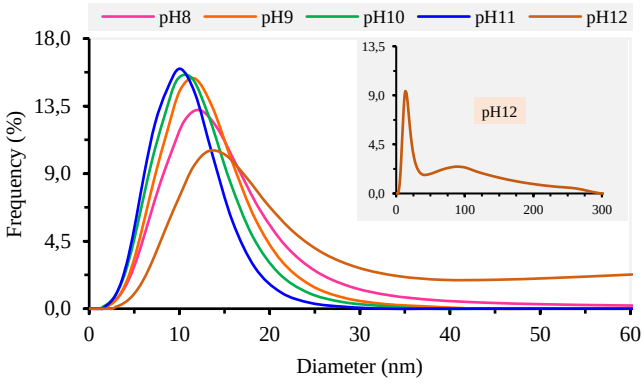

Figure 5. Particle size distribution diagram of AgNPs at pH values

Table 1. Particle size and polydispersity index of AgNPs at different pH values

pH	Z-Average (nm)	PDI
8	11.850 ± 7.487	0.321
9	11.101 ± 4.221	0.284
10	10.666 ± 3.795	0.275
11	10.156 ± 3.615	0.273
12	15.442 ± 42.032	0.896

(PDI: Polydispersity index)

3.4. Nanoparticle morphology

The TEM images of AgNPs at two magnification levels (50,000× and 100,000×), presented in Figure 6, show that the nanoparticles exhibit a spherical or near-spherical shape with a relatively uniform distribution. Some particles tend to aggregate, forming small clusters, which may be attributed to interparticle surface interactions or suboptimal stabilization efficiency. The observed shape and distribution are consistent with the study by Ajitha et al. (2015) in which AgNPs synthesized using Lantana camara leaf extract also exhibited a spherical morphology, with sizes ranging from 10–30 nm. In this study, the authors suggested that polyphenol and flavonoid compounds in the extract played a crucial role in the reduction of silver ions (Ag^+) and nanoparticle stabilization, facilitating the formation of small and uniformly distributed particles [45].

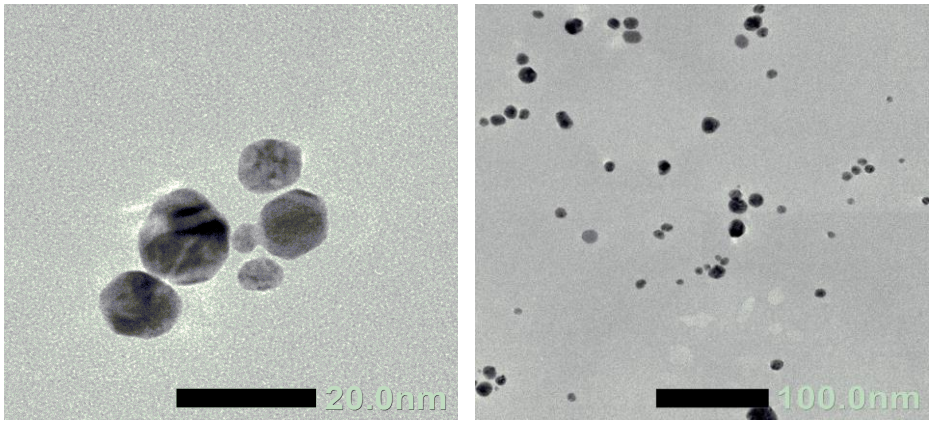

Figure 6. TEM images of AgNPs synthesized at pH 11 value

3.5. Crystallographic properties

The X-ray diffraction (XRD) pattern of AgNPs synthesized using CFE shown in Figure 7, exhibits characteristic diffraction peaks at 2θ ≈ 38.1°, 44.2°, 64.3°,77.4° and 81.6° corresponding to the (111), (200), (220), (311) and (222) crystallographic planes, respectively. These peaks confirm metallic silver's face-centered cubic (FCC) structure, by the JCPDS Card No. 04-0783 for AgNPs. The (111) plane displays the highest intensity, indicating preferential crystal growth along this direction, a common characteristic of AgNPs synthesized using plant extracts. This result is consistent with He et al. findings, where AgNPs were synthesized using *Chrysanthemum morifolium* Ramat. extract exhibited similar diffraction peak positions, further confirming the crystalline stability of the material [26].

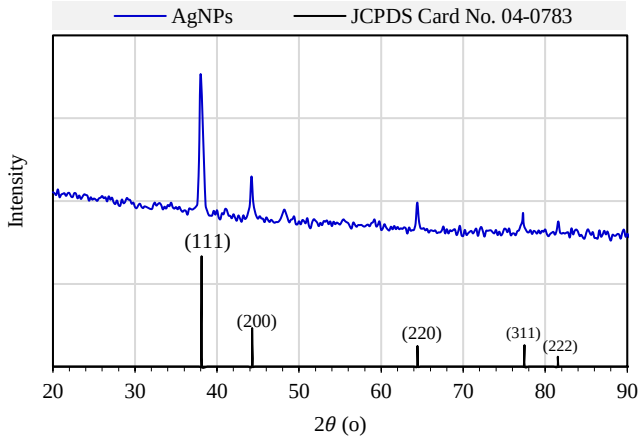

Figure 7. XRD pattern of AgNPs synthesized at pH11 level

The average particle size of AgNPs, calculated using Scherrer's equation, was 10.021 nm, closely matching the mean particle size of 10.156 nm obtained from dynamic light scattering (DLS) measurements. The small discrepancy between these values suggests that the synthesized AgNPs exhibit

high uniformity, with minimal variation in particle size. Scherrer's equation estimates the crystallite size based on the broadening of XRD diffraction peaks, representing the crystalline domain size of AgNPs. In contrast, DLS measurements typically yield slightly larger values, as they account for the hydrodynamic diameter, including the biological capping layer and the dispersion state of nanoparticles in solution. The agreement between these two measurement techniques reinforces the accuracy of XRD-based size estimation and confirms the monodispersity and stability of the synthesized AgNPs. This correlation aligns with the study by Ajitha et al. (2015), where biologically synthesized AgNPs exhibited good agreement between particle sizes obtained from XRD and DLS analyses [45].

3.6. Antibacterial and antifungal activity of AgNPs against *S. aureus* and *C. albicans*

The size of silver nanoparticles (AgNPs) is a key factor influencing their antimicrobial activity, with smaller nanoparticles exhibiting enhanced bactericidal and fungicidal properties due to their larger surface area, which increases the interaction between the nanoparticles and microbial cells [46]. This study selected AgNPs synthesized at pH 11, which exhibited the smallest particle size, to evaluate their antibacterial and antifungal activities. On the other hand, due to their common pathogenicity in skin, mucous membranes, and other environmentally exposed sites, *S. aureus* and *C. albicans* were chosen as representative organisms to evaluate the antibacterial and antifungal activities of biomedical products containing silver nanoparticles, especially in applications such as bandages, antibacterial cosmetics, or antibacterial packaging [33].

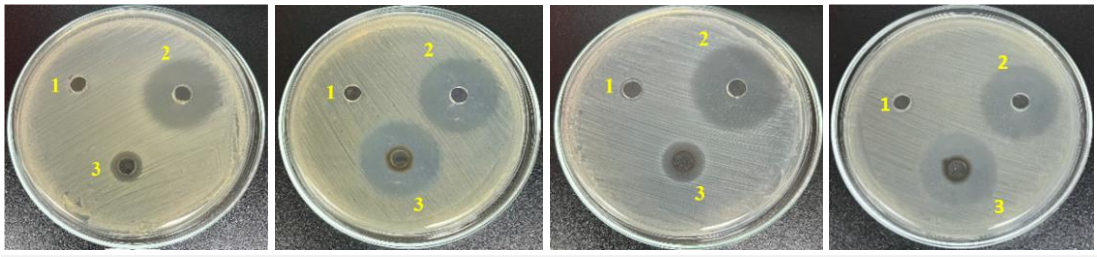

S. aureus-AgNPs 25 ppm | *S. aureus*-AgNPs 100 ppm | *C.albicans*-AgNPs 25 ppm | *C. albicans*-AgNPs 100 ppm

1- Negative control sample; 2- Positive control sample; 3- AgNPs sample

Figure 8. Antibacterial and antifungal activity of AgNPs on agar plates

The results presented in Figure 8 and Table 2 indicate that AgNPs exhibit significant inhibitory effects on both *S. aureus* and *C. albicans*, with the inhibition zone diameter increasing notably as the AgNP concentration increases from 25 ppm to 100 ppm. Specifically, at 25 ppm, the inhibition zone diameter for S. aureus was 8.34 mm, smaller than that for *C. albicans* (13.27 mm). When the AgNPs concentration was increased to 100 ppm, the inhibition zones expanded significantly, reaching 24.82 mm for S. aureus and 28.49 mm for *C. albicans*. These findings suggest that AgNPs exhibit stronger antifungal activity compared to antibacterial activity, which may be attributed to differences in the cell wall structure of Gram-positive bacteria and fungi. Gram-positive bacteria possess a thicker cell wall composed of multiple layers of peptidoglycan, which may reduce the penetration of AgNPs into the cell. In contrast, yeast such as *C. albicans* has a cell membrane rich in ergosterol and chitin, which may interact with AgNPs through a different mechanism, leading to stronger inhibition [33, 47]. Based on these findings, it can be concluded that AgNPs demonstrate significant inhibitory effects against both *S. aureus* and *C. albicans*, with greater efficacy against fungal pathogens. This suggests the potential application of AgNPs in antifungal formulations or surface disinfectants, particularly in medical and cosmetic products.

4. CONCLUSIONS

The study emphasized the important role of pH in the synthesis of AgNPs using *Chrysanthemum morifolium* extract. UV-Vis spectra confirmed the formation of AgNPs, characterized by a surface plasmon resonance (SPR) peak in the range of 405–411 nm, with the best pH in the range of 10–11. TEM and XRD analyses revealed that the AgNPs exhibited a uniform spherical morphology and a face-centered cubic (FCC) crystal structure, with an average crystallite size of 10.021 nm. DLS measurements confirmed that AgNPs synthesized at pH 10–11 possessed small particle sizes (10.156–

10.666 nm) and high stability (PI < 0.3). Antibacterial and antifungal evaluations demonstrated strong inhibitory effects of AgNPs against *S. aureus* and *C. albicans*, two common pathogens that are associated with skin and mucosal infections, with inhibition zone diameters of 24.82 mm and 28.49 mm at 100 ppm, respectively. These results highlight the potential of AgNPs for applications in medical, pharmaceutical, and cosmetic products.

Acknowledgments: This work was financially supported by Ho Chi Minh City University of Industry and Trade under Contract no 60/HD-DCT dated January 7, 2025.

REFERENCES

1. Ahmed S., Ahmad M., Swami B.L., Ikram S. - A review on plants extract mediated synthesis of silver nanoparticles for antimicrobial applications: A green expertise. Journal of Advanced Research **7** (1) (2016) 17-28. https://doi.org/10.1016/j.jare.2015.02.007
2. Chen D., Qiao X., Qiu X., Chen J. - Synthesis and electrical properties of uniform silver nanoparticles for electronic applications. Journal of Materials Science **44** (4) (2009) 1076–1081. https://doi.org/10.1007/s10853-008-3204-y
3. Babu P.J., Tirkey A., Paul A.A., Kristollari K., Barman J., Panda K., Sinha N., Babu B.R., Marks R.S. - Advances in nano silver-based biomaterials and their biomedical applications. Engineered Regeneration **5** (3) (2024) 326-341. https://doi.org/10.1016/j.engreg. 2024.07.001
4. Gowda S., Sriram S. - Green synthesis of chitosan silver nanocomposites and their antifungal activity against *Colletotrichum truncatum* causing anthracnose in chillies. Plant Nano Biology **5** (2023) 100041. https://doi.org/10.1016/j.plana.2023.100041
5. Dell'Annunziata F., Mosidze E., Folliero V., Lamparelli E.P., Lopardo V., Pagliano P., Porta G.D., Galdiero M., Bakuridze A.D., Franci G. - Eco-friendly synthesis of silver nanoparticles from peel and juice *C. limon* and their antiviral efficacy against *HSV-1* and *SARS-CoV-2*. Virus Research **349** (2024) 199455. https://doi.org/10.1016/ j.virusres.2024.199455
6. M., A., Hussian N.N., Mohammed H.A., Aljarbou A., Akhtar N., Khan R.A. - Combined anti-bacterial actions of lincomycin and freshly prepared silver nanoparticles: overcoming the resistance to antibiotics and enhancement of the bioactivity. Antibiotics **11** (12) (2022) 1791. https://doi.org/10.3390/antibiotics11121791
7. More P.R., Pandit S., Filippis A.D., Franci G., Mijakovic I., Galdiero,M. - Silver nanoparticles: Bactericidal and mechanistic approach against drug resistant pathogens. Microorganisms **11** (2) (2023) 369. https://doi.org/10.3390/microorganisms11020369
8. Dipankar C., Murugan S. - The green synthesis, characterization and evaluation of the biological activities of silver nanoparticles synthesized from *Iresine herbstii* leaf aqueous extracts. Colloids and Surfaces B: Biointerfaces **98** (2012) 112-119. https://doi.org/10.1016/j.colsurfb.2012.04.006
9. Niraimathi K.L., Sudha V., Lavanya R., Brindha P. - Biosynthesis of silver nanoparticles using *Alternanthera sessilis (Linn.)* extract and their antimicrobial, antioxidant activities. Colloids and Surfaces B: Biointerfaces **102** (2013) 288-291. https://doi.org/ 10.1016/j.colsurfb.2012.08.041
10. Kalimuthu K., Suresh Babu R., Venkataraman D., Bilal M., Gurunathan S. - Biosynthesis of silver nanocrystals by *Bacillus licheniformis*. Colloids and Surfaces B: Biointerfaces **65** (1) (2008) 150-153. https://doi.org/10.1016 /j.colsurfb.2008.02.018
11. Ingle A., Gade A., Pierrat S., Sonnichsen C., Rai M. - Mycosynthesis of silver nanoparticles using the fungus *Fusarium acuminatum* and its activity against some human pathogenic bacteria. Current Nanoscience 4 (2) (2008) 141-144. https://doi.org/10.2174/157341308784340804
12. Sivalingam P., Antony J.J., Siva D., Achiraman S., Anbarasu K. - *Mangrove Streptomyces sp. BDUKAS10* as nanofactory for fabrication of bactericidal silver nanoparticles. Colloids and Surfaces B: Biointerfaces **98** (2012) 12-17. https://doi.org/10.1016/j.colsurfb.2012.03.032
13. Antony J.J., Sivalingam P., Siva D., Kamalakkannan S., Anbarasu K., Sukirtha R., Krishnan M., Achiraman S. - Comparative evaluation of antibacterial activity of silver nanoparticles synthesized using *Rhizophora apiculata* and glucose. Colloids and Surfaces B: Biointerfaces **88** (1) (2011)

134-140. https://doi.org/10.1016/j.colsurfb.2011.06.022

14. Ahmad S., Munir S., Zeb N., Ullah A., Khan B., Ali J., Bilal M., Omer M., Alamzeb M., Salman S.M., Ali S. - Green nanotechnology: A review on green synthesis of silver nanoparticles - An ecofriendly approach. International Journal of Nanomedicine **2019:14** (2019) 5087-5107. https://doi.org/10.2147/IJN.S200254
15. Ha B.T.T, Anh V.T., Hieu T.B. - Overview of green nano silver synthesis using plant extracts and applications in the pharmaceutical field. VietNam Military Medical Unisversity **47** (2022) 18-29. https://doi.org/10.56535/jmpm.V2022050402
16. Alsammarraie F.K., Wang W., Zhou P., Mustapha A., Lin M. - Green synthesis of silver nanoparticles using turmeric extracts and investigation of their antibacterial activities. Colloids and Surfaces B: Biointerfaces **171** (2018) 398-405. https://doi.org/10.1016/j.colsurfb.2018.07.059
17. Kaviya S., Santhanalakshmi J., Viswanathan B., Muthumary J., Srinivasan K. - Biosynthesis of silver nanoparticles using citrus sinensis peel extract and its antibacterial activity. Spectrochimica Acta Part A: Molecular and Biomolecular Spectroscopy **79** (3) (2011) 594–598. https://doi.org/10.1016/j.saa.2011.03.040
18. Loo Y.Y., Chieng B.W., Nishibuchi M., Radu S. - Synthesis of silver nanoparticles by using tea leaf extract from *Camellia Sinensis*. International Journal of Nanomedicine **7** (2012) 4263-4267. https://doi.org/10.2147/IJN.S33344
19. Devanesan S., Alsalhi M.S. - Green synthesis of silver nanoparticles using the flower extract of *Abelmoschus Esculentus* for cytotoxicity and antimicrobial studies. International Journal of Nanomedicine **16** (2021) 3343-3356. https://doi.org/10.2147/IJN.S307676
20. Su J., Jiang J., Zhang F., Liu Y., Ding L., Chen S., Chen F. - Current achievements and future prospects in the genetic breeding of chrysanthemum: a review. Horticulture Research **6** (2019) 109. https://doi.org/10.1038/s41438-019-0193-8
21. Zhao H.E., Liu Z.H., Hu X., Yin J.L., Li W., Rao G.Y., Zhang X. H., Huang C. L., Anderson N., Zhang Q. X., Chen J. Y. - Chrysanthemum genetic resources and related genera of *Chrysanthemum* collected in China. Genetic Resources and Crop Evolution **56** (2009) 937–946. https://doi.org/10.1007/s10722-009-9412-8
22. Sharma N., Radha, Kumar M., Kumari N., Puri S., Rais N., Natta S., Dhumal S., Navamaniraj N., Chandran D., Mohankumar P., Muthukumar M., Senapathy M., Deshmukh V., Damale R.D., Anitha T., Balamurugan V., Sathish G., Lorenzo J.M. - Phytochemicals, therapeutic benefits and applications of chrysanthemum flower: A review. Heliyon **9** (10) (2023) e20232. https://doi.org/10.1016/j.heliyon.2023.e20232
23. Liu Y.H., Mou X., Zhou D.Y., Zhou D.Y., Shou C.M. - Extraction of flavonoids from *Chrysanthemum morifolium* and antitumor activity in vitro. Experimental and Therapeutic Medicine **15** (2) (2018) 1203–1210. https://doi.org/10.3892/etm.2017.5574
24. Zhang W., Jiang Y., Chen S., Chen F., Chen F. - Concentration-dependent emission of floral scent terpenoids from diverse cultivars of *Chrysanthemum morifolium* and their wild relatives. Plant Science **309** (2021) 110959. https://doi.org/10.1016/j.plantsci. 2021.110959
25. Tymoszuk A., Kulus D. - Silver nanoparticles induce genetic, biochemical, and phenotype variation in chrysanthemum. Plant Cell, Tissue and Organ Culture **143** (2) (2020) 331-344. https://doi.org/10.1007/s11240-020-01920-4
26. He Y., Du Z., Lv H., Jia Q., Tang Z., Zheng X., Zhang K., Zhao F. - Green synthesis of silver nanoparticles by *Chrysanthemum morifolium* Ramat extract and their application in clinical ultrasound gel. International Journal of Nanomedicine **8** (2013) 1809-1815. https://doi.org/10.2147/IJN.S43289
27. Arokiyaraj S., Arasu M.V., Vincent S., Prakash N.U., Choi S.H., Oh Y.K., Choi K.C., Kim K.H. - Rapid green synthesis of silver nanoparticles from *Chrysanthemum indicum L* and its antibacterial and cytotoxic effects: An in vitro study. International Journal of Nanomedicine **9** (1) (2014) 379-388. https://doi.org/10.2147/IJN.S53546
28. Haqq S.M., Pandey H., Gerard M., Chattree A. - Bio-fabrication of silver nanoparticles using *Chrysanthemum coronarium* flower extract and it's in vitro antibacterial activity. International

Journal of Applied Pharmaceutics **10** (5) (2018) 209-213. https://doi.org/10.22159/ijap.2018v10i5.27492

29. Aziz W.J., Jassim H.A. - A novel study of pH influence on Ag nanoparticles size with antibacterial and antifungal activity using green synthesis. World Scientific News **97** (2018) 139-152.
30. Miranda A., Akpobolokemi T., Chung E., Ren G., Raimi-Abraham B.T. - pH alteration in plant-mediated green synthesis and its resultant impact on antimicrobial properties of silver nanoparticles (AgNPs). Antibiotics (Basel) **11** (11) (2022) 1592. https://doi.org/10.3390/antibiotics11111592
31. Briliantama A., Oktaviani N.M.D., Rahmawati S., Setyaningsih W., Palma M. - Optimization of ultrasound-assisted extraction (UAE) for simultaneous determination of individual phenolic compounds in 15 dried edible flowers. Horticulturae **8** (12) (2022) 1216. https://doi.org/10.3390/horticulturae8121216
32. Popov V., Hinkov I., Diankov S., Karsheva M., Handzhiyski Y. - Ultrasound-assisted green synthesis of silver nanoparticles and their incorporation in antibacterial cellulose packaging. Green Processing and Synthesis **4** (2) (2015) 125-131. https://doi.org/ 10.1515/gps-2014-0085
33. Bishoyi A.K., Sahoo C.R., Samal P., Mishra N.P., Jali B.R., Khan M.S., Padhy R.N. - Unveiling the antibacterial and antifungal potential of biosynthesized silver nanoparticles from *Chromolaena odorata* leaves. Scientific Reports **14** 7513 (2024). https://doi.org/ 10.1038/s41598-024-57972-5
34. Sivalingam A.M., Pandian A., Rengarajan S. - Green synthesis of silver nanoparticles using *Vernonia Amygdalina* leaf extract: Characterization, Antioxidant, and Antibacterial Properties. Journal of Inorganic and Organometallic Polymers and Materials **34** (2024) 3212-3228. https://doi.org/10.1007/s10904-024-03046-y
35. Alharbi N.S., Alsubhi N.S., Felimban A.I. - Green synthesis of silver nanoparticles using medicinal plants: Characterization and application. Journal of Radiation Research and Applied Sciences **15** (3) (2022) 109-124. https://doi.org/10.1016/j.jrras.2022.06.012
36. Singh J., Dutta T., Kim K.H., Rawat M., Samddar P., Kumar P. - "Green" synthesis of metals and their oxide nanoparticles: Applications for environmental remediation. Journal of Nanobiotechnology **16** (1) (2018) 1-24. https://doi.org/10.1186/s12951-018-0408-4
37. Asif M., Yasmin R., Asif R., Ambreen A., Mustafa M., Umbreen S. - Green synthesis of silver nanoparticles (AgNPs), structural characterization, and their antibacterial potential. Dose Response **20** (1) (2022) 1-11. https://doi.org/10.1177/15593258221088709
38. Vanlalveni C., Lallianrawna S., Biswas A., Selvaraj M., Changmai B., Rokhum S.L. - Green synthesis of silver nanoparticles using plant extracts and their antimicrobial activities: a review of recent literature. RSC Advances **11** (5) (2021) 2804-2837. https://doi.org/10.1039/D0RA09941D
39. Swilam N., Nematallah K.A. - Polyphenols profile of pomegranate leaves and their role in green synthesis of silver nanoparticles. Scientific Reports **10** (1) (2020) 1-11. https://doi.org/10.1038/s41598-020-71847-5
40. Nurfadhilah M., Nolia I., Handayani W., Imawan C. - The role of pH in controlling size and distribution of silver nanoparticles using biosynthesis from diospyros discolor *Willd. (Ebenaceae)*. IOP Conference Series Materials Science and Engineering **367** (1) (2018) 1-5. https://doi.org/10.1088/1757-899X/367/1/012033
41. Husam M.K. - The effect of pH , temperature on the green synthesis and biochemical activities of silver nanoparticles from *Lawsonia inermis* extract. Journal of Pharmaceutical Sciences and Research **10** (8) (2018) 2022-2026.
42. Sharma V.K., Yngard R.A., Lin Y. - Silver nanoparticles: Green synthesis and their antimicrobial activities. Advances in Colloid and Interface Science **145** (1-2) (2009) 83-96. https://doi.org/10.1016/j.cis.2008.09.002
43. Chandra A., Bhattarai A., Yadav A.K., Adhikari J., Singh M., Giri B. - Green synthesis of silver nanoparticles using tea leaves from three different elevations. ChemistrySelect **5** (14) (2020) 4239-4246. https://doi.org/10.1002/slct.201904826
44. Sun Q., Cai X., Li J., Zheng M., Chen Z., Yu C.P. - Green synthesis of silver nanoparticles using

tea leaf extract and evaluation of their stability and antibacterial activity. Colloids and Surfaces A: Physicochemical and Engineering Aspects **444** (2014) 226-231. https://doi.org/10.1016/j.colsurfa.2013.12.065

45. Ajitha B., Ashok Kumar Reddy Y., Sreedhara Reddy P. - Green synthesis and characterization of silver nanoparticles using *Lantana camara* leaf extract. Materials Science and Engineering: C **49** (2015) 373-381. https://doi.org/10.1016/j.msec. 2015.01.035
46. Secario M.S, Vi T.T.T, Chien-Chang C., Jui-Yang L., Lue S.J. - Size-dependent antibacterial efficacy of silver nanoparticles from a green synthesis method: Effects of extract quantity and origin. Journal of the Taiwan Institute of Chemical Engineers **161** (2024)105511, https://doi.org/10.1016/j.jtice.2024.105511
47. Choi O., Deng K.K., Kim N.J., Ross L., Surampalli R.Y., Hu Z. - The inhibitory effects of silver nanoparticles, silver ions, and silver chloride colloids on microbial growth. Water Research **42** (12) (2008) 3066-3074. https://doi.org/10.1016/j.watres.2008.02.021

TÓM TẮT

TỔNG HỢP XANH NANO BẠC TỪ DỊCH CHIẾT *Chrysanthemum morifolium*: ẢNH HƯỞNG CỦA ĐỘ pH VÀ HOẠT TÍNH KHÁNG KHUẨN, KHÁNG NẤM

Phạm Ngọc Bảo Trâm, Nguyễn Quốc Tuấn, Huỳnh Phước Thông,
Nguyễn Thị Lương, Lê Thị Hồng Thúy*
Trường Đại học Công Thương Thành phố Hồ Chí Minh
*Email: *thuylth@huit.edu.vn*

Bài báo này trình bày nghiên cứu về ảnh hưởng của pH đến quá trình tổng hợp hạt nano bạc (AgNPs) sử dụng dịch chiết hoa *Chrysanthemum morifolium* (CFE) làm chất khử, đồng thời đánh giá hoạt tính kháng khuẩn và kháng nấm của AgNPs tại điều kiện pH tối ưu. Phổ hấp thụ UV-Vis cho thấy đỉnh cộng hưởng plasmon bề mặt (SPR) đặc trưng trong khoảng bước sóng 405–411 nm, với cường độ hấp thụ mạnh nhất tại pH 11. Kết quả phân tích bằng phương pháp tán xạ ánh sáng động (DLS) chỉ ra rằng AgNPs được tổng hợp tại pH 10–11 có kích thước hạt nano nhỏ nhất (10,156–10,666 nm) và chỉ số phân tán PDI< 0,3, chứng tỏ hệ hạt có tính ổn định cao và phân bố kích thước đồng đều. Phân tích TEM và XRD xác nhận AgNPs có hình cầu và cấu trúc tinh thể dạng lập phương tâm mặt (FCC), với kích thước tinh thể trung bình là 10,021 nm. Đánh giá hoạt tính kháng khuẩn và kháng nấm cho thấy AgNPs có tác dụng ức chế mạnh đối với *Staphylococcus aureus* và *Candida albicans*, hai tác nhân gây bệnh phổ biến ở da và niêm mạc, với đường kính vòng ức chế lần lượt là 24,82 mm và 28,49 mm ở nồng độ 100 ppm. Những kết quả này khẳng định tiềm năng ứng dụng của AgNPs trong lĩnh vực y học, dược phẩm và mỹ phẩm.

Từ khóa: Hạt nano bạc, *Chrysanthemum morifolium*, tổng hợp xanh, hoạt tính kháng khuẩn, hoạt tính kháng nấm.